Thermal relaxation in NbN films on crystalline substrates

E.M. Baeva, M.D. Soldatenkova, P.I. Zolotov, N.A. Titova, A.D. Triznova, A.I. Lomakin, A.I. Kardakova, and G.N. Goltsman

***Abstract*—Here we focus on thermal transport in NbN films, deposited on crystalline substrates. Using the noise thermometry, we found that thermal relaxation in thin NbN films at temperatures above the critical superconducting temperature is mainly restricted by the thermal boundary resistance, and it can be modified by a structural disorder on a substrate surface. In addition, for thick NbN films deposited on a sapphire substrate, we also observe that thermal relaxation occurs in the diffusive phonon regime when the phonon mean free path is shorter than the film thickness. The findings can be exploited for low-temperature devices based on NbN films.**

***Index Terms*—superconducting thin films, thermal boundary resistance, low-temperature detectors, phonon mean free path.**

I. Introduction

THERMAL properties of thin metallic layers have an outsized impact on efficiency and sensitivity of devices with nanoscale structures, such as superconducting single-photon detectors [1], superconducting thermal switches [2], hot-electron [3] and microwave bolometers [4]. Typically, thermal transport in thin-film devices is determined by microscopic processes such as electron-electron (e-e) and electron-phonon (e-ph) interactions, and phonon scattering at sample boundaries. For instance, in devices based on one of the conventional superconducting materials, niobium nitride (NbN), e-e and e-ph scatterings occur rapidly [5], that is why a bottleneck in thermal transport is often associated with the passage of phonons through the film-substrate interface, so-called the Kapitza resistance [6], [7]. The aforementioned thermalization process in NbN films plays a key role in the operating parameters of devices, such as the response time of bolometers [7], the intermediate frequency bandwidth of mixers [6], quantum efficiency, latency, and jitter of superconducting single-photon detectors [8], [9]. However, recent studies of the thermal properties of various NbN devices pose further challenges. First of all, experimental values of the phonon escape time from the NbN film to the substrate, τ_{esc}, are shown to be more than one order of magnitude longer than the ballistic phonon time of flight across the film thickness d/v_s [5], [10], [7], where d and v_s are thickness and sound velocity, respectively. To explain this difference, it has been shown recently that the magnitude of τ_{esc} is determined by the angle-dependent transmission coefficient of phonons through the film-substrate interface [11], [12]. If the incident angle of the phonon is larger than the critical angle, the phonon cannot escape the film, increasing τ_{esc} to infinity. Further studies also show that the phonon spectrum in a thin film cannot be considered isotropic, and, in result, it causes suppression of the phonon density of states and a two-time decrease of the sound velocity [5]. Other heat flow restriction mechanisms are revealed in NbN devices embedded into amorphous substrates, where the thermal bottleneck is established due to low thermal conductance of amorphous substrate characterized by the short phonon mean free path l_{ph} [13], [14], [15]. The common feature of these experiments is that the heat transport is considered under the Casimir limit, which implies that the bulk NbN phonon mean free path l_{ph} is larger than d. However, when the strong e-ph interaction and, hence, the strong phonon-electron scattering are inherent for the film material, the magnitude of l_{ph} is under question.

Here we present our study of the heat flow rate in NbN films deposited on various crystalline substrates. The heat flow rate from electrons to thermal bath measured above superconducting critical temperature T_c can be described with the power dependence $P_{2D} = \Sigma_{2D}(T_e^n - T_b^n)$, where P_{2D} is the Joule heat normalized on the sample area, Σ_{2D} is the cooling rate, n is the exponent, T_e and T_b are the electron and bath temperatures. To compare our experimental results with existing theories, we derive the effective thermal conductance $G_{2D} = dP_{2D}/dT_e$. For thin NbN films with $d \leq 7\,\text{nm}$, we observe that G_{2D} is quantitatively close to the thermal boundary conductance G_K, but its temperature dependence differs from the expected $G_K(T)$. With temperature increasing, the discrepancy between G_{2D} and G_K also increases, which can be attributed to substrate-mediated effects [13], [14], [15]. For the NbN samples on sapphire substrate, we find that G_{2D} is less influenced by the substrate effects than the values obtained for the other substrates. In addition, we study thermal relaxation in NbN films on sapphire substrates as a function of thickness, with d from 5 nm up to 300 nm. At increasing d, we observe G_{2D} decreases. This behavior is a hallmark of the diffusive regime, which implies the condition $l_{ph} \ll d$. This condition also results in the gradient of T_e established across the film thickness [16]. The observed $G_{2D}(d)$-dependence allows to estimate the phonon thermal conductivity κ_{ph} and l_{ph} in bulk NbN.

This work was supported by the Russian Science Foundation project No.19-72-10101.

E.M. Baeva, M.D. Soldatenkova, A.I. Triznova, A.I. Lomakin, A.I. Kardakova, and G.N. Goltsman are with National Research University Higher School of Economics, Moscow 101000, Russia and also Moscow Pedagogical State University, Moscow 119021, Russia(e-mail: baeva.elm@gmail.com.).

P.I. Zolotov is with National Research University Higher School of Economics, Moscow 101000, Russia, and with LLC Superconducting Nanotechnology (SCONTEL), Moscow 119021, Russia.

N.A. Titova is with Moscow Pedagogical State University, Moscow 119991, Russia.

Manuscript received ; revised .

II. Samples and Experimental Methods

Disordered NbN films are deposited by DC reactive magnetron sputtering onto crystalline substrates. The 4.7-nm NbN film is deposited on the gallium nitride (GaN) substrate[1] at heating temperature of 500 °C. The 7 and 50-nm NbN films are deposited at room temperature on 400-μm thick Si substrate with 1-2 nm thick native oxide layer (SiO_2). The set of NbN films of thicknesses from 5 nm to 300 nm are deposited on the 300-μm thick sapphire (Al_2O_3) substrate at 400 °C. In Figure 1(a), we plot the atomic-force-microscope (AFM) images of the substrates. We believe that completely different conditions for the film deposition and the choice of the substrate provide an astounding variety of morphology, which is reflected in the level of the disorder of NbN films. Thicknesses of the films are determined from deposition time with a calibrated quartz crystal. After deposition, the films are patterned into two-contact bridges using conventional UV photolithography and thermal evaporation of Ti/Au contact pads followed by plasma-chemical etching. The parameters of films (the thickness d, T_c determined at $R = R_n/2$) and the parameters of samples (the length L, the width w, and the normal-state resistance R_n at 20 K) are listed in Table I.

TABLE I
The Parameters of NbN Samples

Sub.	d (nm)	T_c (K)	$w \times L$ (μm×μm)	R_n (kΩ)	n	$\Sigma_{2D} \times 10^2$ (W/K^{n}m^2)	$G_{2D}^{20K} \times 10^6$ (W/Km^2)
GaN	4.7	13.7	0.9×10	3.3	3	2.2	2.7
			2.7×7.3	1.5	3	1.7	2
			$0.5 \times 8^*$	4.7	3	1.8	2.2
Si	7	8	$0.48 \times 3.9^*$	9.7	3	20	2.4
	50	11.7	1×25.6	4.4	3	23	2.8
Al_2O_3	5	11.7	$0.5 \times 8^*$	9.7	4	2.1	6.9
			0.5×3	4.5	4	2	6.6
			0.5×1.5	3.5	4	2	6.6
	10	12.6	0.5×17	6.2	4	1.8	5.9
			0.5×7	2.8	4	2	6.5
	30	13.2	0.5×45	6.9	3.8	3.4	5.7
			0.4×18	2.9	3.8	3.3	5.6
	50	12.9	0.6×67	5.4	3	49	5.8
			1×54	2.3	3	39	4.7
	100	13.3	0.5×120	5.9	3	40	4.9
			0.5×48	2.5	3	41	5
	200	14	0.5×95	3.2	3	29	3.5
			1×94	1.4	3	23	2.7
	300	13.9	0.35×64	2.2	3	19	2.2
			0.35×64	2	3	18	2.1
			0.95×243	2.9	3	14	1.7

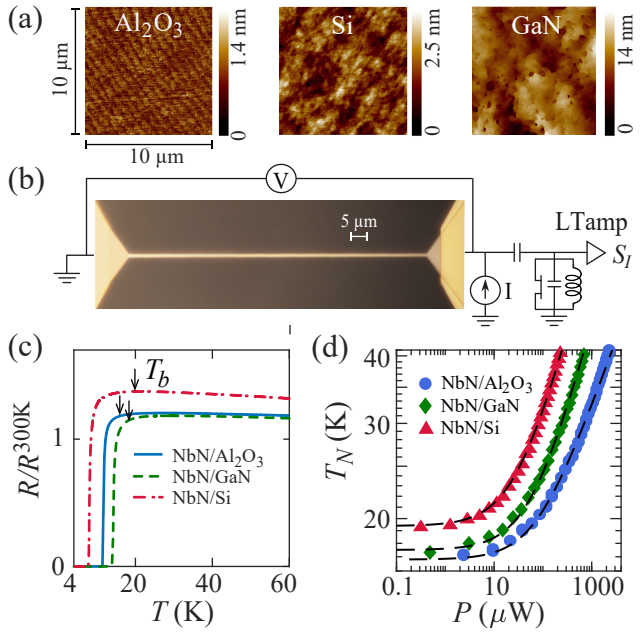

Fig. 1. (a) AFM images of substrate surfaces is obtained in classical contact mode. The rms roughness of the surfaces is 0.2 nm for Al_2O_3, 0.4 nm for Si, and 2 nm for GaN, respectively. (b) Optical image of a representative device and the schematic of the experimental methods. (c) Temperature dependence of resistance normalized on value at 300 K. (d) The heat flow rate for NbN samples marked in Table I with $*$-symbol. The values of bath temperature T_b are marked with arrows.

The optical image of a representative sample is presented in Figure 1(b). The temperature dependencies of the normalized resistance (R/R^{300K}) for thin (5-7-nm thick) NbN films, deposited on three types of substrates, are shown in Figure 1(c). We observe that R increases at decreasing T from 300 K to 20 K and drops to zero at T_c. Such behavior is usually prescribed to effects of the weak localization and e-e interactions on resistivity in the disordered NbN films [17], [18]. At room temperature, where these mechanisms are weak, the resistivity ρ reflects a level of disorder [18], which is also responsible for superconductivity suppression in the disordered NbN films [19]. We find consistency in qualitative values of ρ ($\rho = 208 \pm 20\,\mu\Omega$cm for NbN/$Al_2O_3$ films, 173 $\mu\Omega$cm for NbN/GaN films, $550 \pm 10\,\mu\Omega$cm for NbN/Si films) and T_c with this mechanism.

In order to study the heat flow rate, we measure the noise temperature T_N [20], which reflects the average electron temperature T_e in the sample. Figure 1(b) shows the schematic of the experimental setup. The sample biased with the dc current I produces the excess current noise. The noise signal, passed through the resonance tank circuit at a central frequency of 46 MHz, is amplified by a homemade low-temperature amplifier (LTamp), with the 6-dB gain and the input current noise of $10^{-27}\,A^2/Hz$, and the chain of room-temperature amplifiers with the 75-dB gain and measured by a power detector. Calibrating the circuit with the Johnson-Nyquist noise [21], we extract the current noise of the sample S_I. Here T_N can be found using the Johnson-Nyquist formula $T_N = S_I R_d / 4k_B$, where k_B is the Boltzmann constant. The change in the differential resistance of the sample R_d with current is within 10%.

III. Results and Discussion

Figure 1 (d) displays the dependencies of T_N on the Joule power P for samples on various substrates (shown with symbols). At low heating, T_N is close to T_b, which is usually chosen to be above T_c in the experiment. At intense heating, we observe the power dependence $P \propto T_N^n$. For further analysis, we fit our experimental data with the power-law

[1]GaN layer was deposited with an underlying buffer layers over the high-resistivity Si wafer. The layout was as follows (from top to bottom): GaN(450 nm)/$Al_{0.2}$GaN(150 nm)/$Al_{0.5}$GaN(150 nm)/AlN(100 nm)/Si(350 μm)

dependence $P_{2D} = \Sigma_{2D}\,(T_e^n - T_b^n)$ shown with the dashed lines. Table I gives an overview of the fitting parameters for the studied samples: Σ_{2D} and n. Since n and hence the unit of measure for Σ_{2D} differs for different samples, it is convenient to compare the experimental data using the magnitude of G_{2D}. As one can see, the derived value of G_{2D} at $T \equiv T_N = 20\,\mathrm{K}$ for NbN/GaN samples is surprisingly close to G_{2D} for NbN/Si samples, despite the different levels of disorder of NbN films. Similar value of G_{2D} (at $n = 4$) extrapolated to $T = 20\,\mathrm{K}$ has been reported for NbN/Si interface [22]. However, for NbN/Al_2O_3 interface we observe that G_{2D} is three times higher than the values derived for NbN/GaN and NbN/Si samples and for NbN/Al_2O_3 interface reported in Ref. [22].

To analyze experimental results we compare temperature dependence of G_{2D} with both e-ph thermal conductance G_{e-ph} and G_K in Figure 2. As follows from the heat balance equations (see Eq.(1)-(2) in the Appendix), G_{2D} is defined by the lowest thermal conductance among G_K and G_{e-ph}, which have the following temperature trends $G_{e-ph} \propto T^4$ and $G_K \propto T^3$ [23]. In the temperature range of our experiment, $G_K \ll G_{e-ph}$, and therefore we expect that G_K determines the total thermal conductance. As expected, the experimental values of G_{2D} for thin films are much lower than G_{e-ph}, but rather close to G_K. Also, the temperature dependence of G_{2D} at $T < 30\,\mathrm{K}$ resembles the T-trend specific for G_K, and deviates slightly from it at T above 30 K.

Upon increasing temperature, the discrepancy between G_{2D} and G_K becomes more pronounced and can be associated with two different substrate effects, the first of which arises due to the diffusion phonon regime in the substrate [13], [14], [15]. To assess the contribution of the effect we estimate $l_{ph} = 3\kappa_{ph}/v_s C_{ph}$ (l_{ph} >150 μm for Si and Al_2O_3 [24], [25] and l_{ph} >0.5 μm for GaN [26] in the 10 K-40 K temperature range) in the exploited substrates, where C_{ph} is the phonon specific heat capacity. Our estimations of l_{ph} crucially differ from l_{ph} in SiO_2 ($l_{ph} \simeq 4.5\,\mathrm{nm}$ at 10 K) [15], and we believe that this effect cannot take place here. Note, we do not take into account the native SiO_2 layer on top of the Si substrate, since its thickness is less than l_{ph} for SiO_2. In addition, we observe that G_{2D} for NbN samples on amorphous SiO_2(300 nm)/Si [15] substrate (black dashed line) is significantly lower than G_{2D} for samples on crystalline substrates. The second substrate effect, which is related to the structural disorder on the surface, can explain the deviation of G_{2D} from G_K at T above 30 K. This structural surface disorder can cause the efficient scattering of high-frequency phonons, and thus can lead to the weaker T-trend of G_{2D} [24]. Since the Si and GaN substrates have high surface roughness (see Figure 1(a)), the mechanism could be responsible for the lower values of G_{2D} observed for NbN/Si and NbN/GaN samples.

Next, for the samples on the sapphire substrate, for which the observed deviation between G_{2D} and G_K is minimal, we investigate the transition of the thermal relaxation from the ballistic to the diffusion phonon regime. We observe that G_{2D} decreases with increasing d and the T-trend of $G_{2D} \propto T^{n-1}$ changes from $n = 4$ to $n = 3$. In Figure 3 we plot G_{2D} obtained at 20 K for all studied NbN/Al_2O_3 samples versus d; the same trend is also observed at other temperatures (not shown here). The observed monotonic decrease of G_{2D} with an increase in d contrasts sharply with the trends expected for the e-ph and thermal boundary conductances ($G_{e-ph} \propto d$ and $G_{2D} \propto$const) and can be explained by considering the diffusive phonon regime in NbN film.

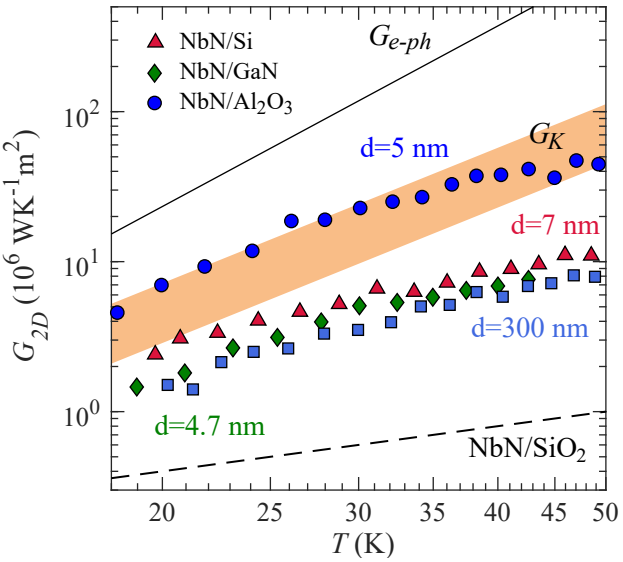

Fig. 2. Measured thermal conductance G_{2D} as a function of T, for the NbN samples deposited on GaN, Al_2O_3, Si, and SiO_2/Si [15] in comparison with G_{e-ph} and G_K. The estimation of G_K in frames of acoustic and diffusive mismatch models for NbN/GaN, NbN/Si, and NbN/Al_2O_3 interfaces covers orange region.

In the diffusive phonon regime, the temperature gradient across the film thickness is established (see the inset of Figure 3 and the Appendix for details). From the heat balance equations in the diffusive phonon regime, the thermal conductance can be determined as $G_{grad} \propto \kappa(T)/d$, where $\kappa(T) = \kappa_e + \kappa_{ph}$ is the total thermal conductivity of the NbN film. Below, we explore the temperature dependence of κ in NbN films. In the inset of Figure 3 one can see the thickness trends expected for G_K, G_{grad}, and total thermal conductance $G_{tot}^{-1} = G_K^{-1} + G_{grad}^{-1}$. Note that G_{grad} manifests itself in G_{2D} if the effective thermal conductance mediated by substrate effects is low enough, as observed in NbN/Al_2O_3 samples. Fitting the experimental data with G_{tot} (see black dashed line in Figure 3) we obtain the parameters $\Sigma_K = 214 \pm 15\ \mathrm{WK^{-4}m^{-2}}$ and $\kappa = 0.22$ W/Km at 20 K. Taking into account κ_e given by the Wiedemann-Franz law $\kappa_e = \mathcal{L}\rho^{-1}T \simeq 0.15$ W/Km, where $\mathcal{L}$ is the Lorenz number, we estimate $\kappa_{ph} \simeq 0.06$ W/Km in NbN at 20 K. The $\kappa_e \gg \kappa_{ph}$ scenario can be relevant for the strong e-ph interaction in NbN [16], as well as other phonon scattering mechanisms [27]. In the phonon diffusion regime, the exponent $n = 3$ observed for the 50-300-nm thick NbN films indicates that $\kappa_e(T) + \kappa_{ph}(T) \propto T^2$ with $\kappa_{ph}(T) \propto T^{2.7}$. Since the T-trend for $\kappa_{ph}(T)$ is close to the T-trend for $C_{ph}(T)$ from the Debye model, we believe that l_{ph} has the weak T-dependence. Taking into account value of C_{ph} and v_s for bulk NbN [28] we estimate $l_{ph} = 4\,\mathrm{nm}$ at $T = 20$ K. The similar estimate $l_{ph} \simeq 1.4\,\mathrm{nm}$ at $T = 20$ K can be obtained considering the reduced v_s and phonon density of states in

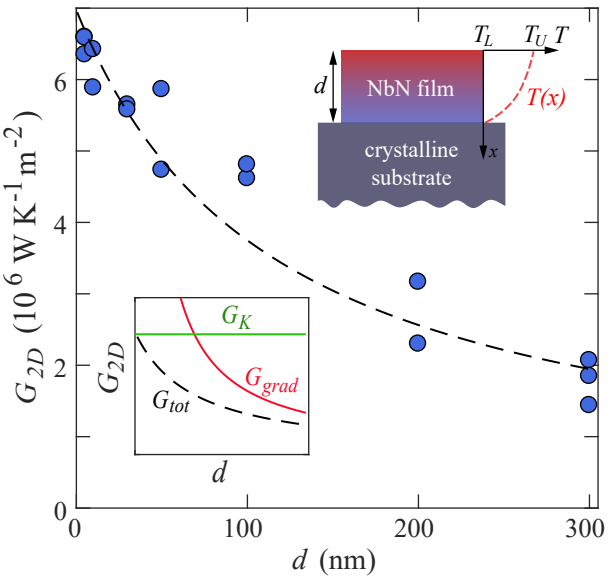

Fig. 3. Main: Thickness dependence of the thermal conductance G_{2D} at 20 K for NbN samples deposited on Al_2O_3 substrate. The right inset shows the thermal relaxation in a thick metal film deposited on a crystalline substrate leads to a temperature gradient across the film in the x-direction. The left inset shows the schematic contribution of G_K and G_{grad} into total thermal conductance G_{tot} of the film.

the 30-nm NbN film [5]. For more disordered NbN films one can expect a lower value of κ, and hence, shorter value of l_{ph}. These observations highlight that it is more difficult to achieve the Casimir limit than it is assumed for devices based on NbN films [29], [30], [2], [31]. Moreover, we note the value of l_{ph} is close to the dominant phonon wavelength $\lambda_{ph} \simeq 4$ nm at T=20 K, defined as $\lambda_{ph} = hv_s/2.82k_BT$ [32]. This finding demonstrates that the phonon transport in NbN films can be unusual due to proximity to the Ioffe-Regel threshold value ($l_{ph} = \lambda_{ph}/2$), and it can be interesting for the further fundamental research of thermal transport in disordered films.

Performance of low-temperature devices based on NbN superconducting films are generally believed to be restricted by the thermal boundary conductance between the NbN film and the substrate [22]. However, we identify two more mechanisms, both of which restricts the thermal relaxation in NbN films. The first of them, related to the surface disorder on top of substrate [24], can be eliminated by the right treatment of the substrate surface. The second one related to the phonon diffusive regime in NbN can be reduced by decreasing the film thickness. According to our results, both mechanisms should be taken into account in modeling of the thermal performance of various low-temperature devices based on the disordered NbN films.

IV. Conclusion

In conclusion, we investigate the thermal properties of NbN films on the different crystalline substrates at $T > T_c$. For thin films ($\leq$7 nm) we observe that the effective thermal conductance of NbN film is limited by the Kapitza thermal resistance or the disorder on the substrate surface. Further increasing the film thickness for NbN films deposited on sapphire substrate allows to explore the phonon diffusive regime in NbN and to derive l_{ph} in thick NbN films. Thus, we show two more mechanisms that can limit thermal performance of low-temperature NbN devices besides the Kapitza resistance.

Appendix

In the two-temperature model, the electron T_e and the phonon T_{ph} temperatures at the normal state of NbN can be obtained from the coupled heat balance equations:

$$\nabla\kappa_e\left(\nabla T_e\right) = -P_{2D}/d + \Sigma_{e-ph}\left(T_e^5 - T_{ph}^5\right) \quad (1)$$

$$\nabla\kappa_{ph}\left(\nabla T_{ph}\right) = -\Sigma_{e-ph}\left(T_e^5 - T_{ph}^5\right) + \frac{\Sigma_K}{d}\left(T_{ph}^4 - T_b^4\right) \quad (2)$$

where Σ_{e-ph} is the e-ph coupling constant, κ_e is the electron thermal conductivity, κ_{ph} is the phonon thermal conductivity, and Σ_K describes the phonon emissivity between the NbN film and the substrate. Here, it is instructive to estimate the e-ph scattering length $l_{e-ph} = \sqrt{\tau_{e-ph}D}$. Using the e-ph time in NbN $\tau_{e-ph} \simeq 2.5T^{-3}$ ns [5] and the electron diffusivity $D = 0.3-0.5$ cm^2/s, we estimate $l_{e-ph} \simeq 1.3$ nm at 20 K. The configuration of our samples ($L \gg l_{e-ph}$) implies uniformity of T_e along the sample length L. Under the Casimir limit ($\nabla T_{ph} = 0$), the solution of Eq.(1)-(2) is simplified. Here it is convenient for analysis to express the solution in terms of the total thermal conductance as $G_{tot}^{-1} \equiv dT/dP_{2D} = G_K^{-1} + G_{e-ph}^{-1}$, where G_{e-ph} is e-ph conductance and G_K is the thermal boundary conductance. The e-ph conductance can be estimated as $G_{e-ph} = dC_e/\tau_{e-ph}$, where C_e is specific heat capacity of electrons. According to the model of free electron gas, $C_e = \pi^2 N_0 k_B^2 T/3$, where $N_0 = \left(\rho e^2 D\right)^{-1}$ is density of states at Fermi level. The thermal boundary conductance in analogy to the Stefan-Boltzmann law can be found as $G_K = 4\Sigma_K T^3$, where the value of Σ_K is calculated using the acoustic and diffuse mismatch models (AMM and DMM) in ref. [22]. The temperature dependencies of G_K for all interfaces and G_{eph} are shown in Fig. 2.

In the thick film limit ($d \gg l_{ph}$), Eq.(1)-(2) are simplified to:

$$d\frac{\partial}{\partial x}\left(\kappa\frac{\partial T}{\partial x}\right) = -P_{2D} \quad (3)$$

According to ref. [16], the substitution of $\kappa(T) \propto T^{n-1}$ into Eq.(3) leads to the solution for the spatial T-profile $T^n(x) = T_U^n - (T_U^n - T_L^n)\,x^2/d^2$ and the relation $P_{2D} \propto T_N^n$. Here T_U and T_L are temperatures at the upper and lower surfaces of the NbN film (see Figure 3(a)), and $T_N = d^{-1}\int T(x)dx$ is the averaged temperature. To compare experimental results with measured G_{2D}, we derive the thermal conductance due to the spatial T-profile along x-axes $G_{grad} = 2(4/\pi)^n\kappa(T)/d$ in the limit of $T_U \gg T_L$. In inset of Figure 3 we schematically plot the d-dependencies of G_K, G_{grad}, and total thermal conductance $G_{tot}^{-1} = G_K^{-1} + G_{grad}^{-1}$.

Acknowledgment

The authors would like to acknowledge V.S. Khrapai for useful discussion of the work and LLC Sigm Plus for fabrication of GaN test substrates.

REFERENCES

[1] D. Y. Vodolazov, "Single-photon detection by a dirty current-carrying superconducting strip based on the kinetic-equation approach," *Phys. Rev. Applied*, vol. 7, p. 034014, Mar 2017.

[2] R. Baghdadi, J. P. Allmaras, B. A. Butters, A. E. Dane, S. Iqbal, A. N. McCaughan, E. A. Toomey, Q.-Y. Zhao, A. G. Kozorezov, and K. K. Berggren, "Multilayered heater nanocryotron: A superconducting-nanowire-based thermal switch," *Phys. Rev. Applied*, vol. 14, p. 054011, Nov 2020.

[3] F. Giazotto, T. T. Heikkilä, A. Luukanen, A. M. Savin, and J. P. Pekola, "Opportunities for mesoscopics in thermometry and refrigeration: Physics and applications," *Rev. Mod. Phys.*, vol. 78, pp. 217–274, Mar 2006.

[4] R. Kokkoniemi, J. Govenius, V. Vesterinen, R. E. Lake, A. M. Gunyhó, K. Y. Tan, S. Simbierowicz, L. Grönberg, J. Lehtinen, M. Prunnila, J. Hassel, A. Lamminen, O.-P. Saira, and M. Möttönen, "Nanobolometer with ultralow noise equivalent power," *Communications Physics*, vol. 2, Oct. 2019.

[5] M. Sidorova, A. Semenov, H.-W. Hübers, K. Ilin, M. Siegel, I. Charaev, M. Moshkova, N. Kaurova, G. N. Goltsman, X. Zhang, and A. Schilling, "Electron energy relaxation in disordered superconducting nbn films," *Phys. Rev. B*, vol. 102, p. 054501, Aug 2020.

[6] S. Krause, V. Mityashkin, S. Antipov, G. Gol'tsman, D. Meledin, V. Desmaris, V. Belitsky, and M. Rudziński, "Reduction of phonon escape time for nbn hot electron bolometers by using gan buffer layers," *IEEE Transactions on Terahertz Science and Technology*, vol. 7, no. 1, pp. 53–59, 2017.

[7] S. Cherednichenko, V. Drakinskiy, J. Baubert, J.-M. Krieg, B. Voronov, G. Gol'tsman, and V. Desmaris, "Gain bandwidth of NbN hot-electron bolometer terahertz mixers on 1.5μm Si_3N_4/SiO_2 membranes," *Journal of Applied Physics*, vol. 101, p. 124508, June 2007.

[8] Y. Ota, K. Kobayashi, M. Machida, T. Koyama, and F. Nori, "Direct numerical simulation for non-equilibrium transport phenomena in superconducting detectors," *Physics Procedia*, vol. 27, pp. 352–355, 2012.

[9] J. Allmaras, A. Kozorezov, B. Korzh, K. Berggren, and M. Shaw, "Intrinsic timing jitter and latency in superconducting nanowire single-photon detectors," *Phys. Rev. Applied*, vol. 11, p. 034062, Mar 2019.

[10] R. P. S. M. Lobo, J. D. LaVeigne, D. H. Reitze, D. B. Tanner, Z. H. Barber, E. Jacques, P. Bosland, M. J. Burns, and G. L. Carr, "Photoinduced time-resolved electrodynamics of superconducting metals and alloys," *Phys. Rev. B*, vol. 72, p. 024510, Jul 2005.

[11] S. B. Kaplan, "Acoustic matching of superconducting films to substrates," *Journal of Low Temperature Physics*, vol. 37, pp. 343–365, Nov. 1979.

[12] M. V. Sidorova, A. G. Kozorezov, A. V. Semenov, Y. P. Korneeva, M. Y. Mikhailov, A. Y. Devizenko, A. A. Korneev, G. M. Chulkova, and G. N. Goltsman, "Nonbolometric bottleneck in electron-phonon relaxation in ultrathin wsi films," *Phys. Rev. B*, vol. 97, p. 184512, May 2018.

[13] E. T. Swartz and R. O. Pohl, "Thermal resistance at interfaces," *Appl. Phys. Lett.*, vol. 51, pp. 2200–2202, Dec. 1987.

[14] J. P. Allmaras, A. G. Kozorezov, A. D. Beyer, F. Marsili, R. M. Briggs, and M. D. Shaw, "Thin-film thermal conductivity measurements using superconducting nanowires," *Journal of Low Temperature Physics*, vol. 193, pp. 380–386, July 2018.

[15] E. M. Baeva, N. A. Titova, L. Veyrat, B. Sacépé, A. V. Semenov, G. N. Goltsman, A. I. Kardakova, and V. S. Khrapai, "Thermal relaxation in metal films limited by diffuson lattice excitations of amorphous substrates," *Phys. Rev. Applied*, vol. 15, p. 054014, May 2021.

[16] E. M. Baeva, N. A. Titova, A. I. Kardakova, S. U. Piatrusha, and V. S. Khrapai, "Universal bottleneck for thermal relaxation in disordered metallic films," *JETP Lett.*, vol. 111, p. 104, Jan. 2020.

[17] Y. Pellan, G. Dousselin, J. Pinel, and Y. U. Sohn, "Temperature and magnetic field dependence of NbN film resistivity: 3d weak localization effects," *Journal of Low Temperature Physics*, vol. 78, pp. 63–77, Jan. 1990.

[18] M. Chand, A. Mishra, Y. M. Xiong, A. Kamlapure, S. P. Chockalingam, J. Jesudasan, V. Bagwe, M. Mondal, P. W. Adams, V. Tripathi, and P. Raychaudhuri, "Temperature dependence of resistivity and hall coefficient in strongly disordered nbn thin films," *Phys. Rev. B*, vol. 80, p. 134514, Oct 2009.

[19] B. Sacépé, M. Feigel'man, and T. M. Klapwijk, "Quantum breakdown of superconductivity in low-dimensional materials," *Nature Physics*, vol. 16, pp. 734–746, July 2020.

[20] M. L. Roukes, M. R. Freeman, R. S. Germain, R. C. Richardson, and M. B. Ketchen, "Hot electrons and energy transport in metals at millikelvin temperatures," *Phys. Rev. Lett.*, vol. 55, pp. 422–425, Jul 1985.

[21] E. S. Tikhonov, M. Y. Melnikov, D. V. Shovkun, L. Sorba, G. Biasiol, and V. S. Khrapai, "Nonlinear transport and noise thermometry in quasiclassical ballistic point contacts," *Phys. Rev. B*, vol. 90, p. 161405, Oct 2014.

[22] A. Dane, J. Allmaras, D. Zhu, M. Onen, M. Colangelo, R. Bahgdadi, J.-L. Tambasco, Y. Morimoto, I. E. Forno, I. Charaev, Q. Zhao, M. Skvortsov, A. Kozorezov, and K. Berggren, "Self-heating hotspots in superconducting nanowires cooled by phonon black-body radiation," 2021.

[23] F. C. Wellstood, C. Urbina, and J. Clarke, "Hot-electron effects in metals," *Phys. Rev. B*, vol. 49, pp. 5942–5955, Mar 1994.

[24] E. T. Swartz and R. O. Pohl, "Thermal boundary resistance," *Rev. Mod. Phys.*, vol. 61, pp. 605–668, Jul 1989.

[25] D. G. Cahill and R. O. Pohl, "Lattice vibrations and heat transport in crystals and glasses," *Annual Review of Physical Chemistry*, vol. 39, pp. 93–121, Oct. 1988.

[26] M. E. Levinshtein, *Properties of advanced semiconductor materials : GaN, AlN, InN, BN, SiC, SiGe*. New York: Wiley, 2001.

[27] M. Asheghi, K. Kurabayashi, R. Kasnavi, and K. E. Goodson, "Thermal conduction in doped single-crystal silicon films," *Journal of Applied Physics*, vol. 91, pp. 5079–5088, Apr. 2002.

[28] D.-H. Ren and X.-L. Cheng, "First-principles calculations on the elastic and thermodynamic properties of NbN," *Chinese Physics B*, vol. 21, p. 127103, Dec. 2012.

[29] A. Tavakoli, C. Blanc, H. Ftouni, K. J. Lulla, A. D. Fefferman, E. Collin, and O. Bourgeois, "Universality of thermal transport in amorphous nanowires at low temperatures," *Phys. Rev. B*, vol. 95, p. 165411, Apr 2017.

[30] T. Nguyen, A. Tavakoli, S. Triqueneaux, R. Swami, A. Ruhtinas, J. Gradel, P. Garcia-Campos, K. Hasselbach, A. Frydman, B. Piot, M. Gibert, E. Collin, and O. Bourgeois, "Niobium nitride thin films for very low temperature resistive thermometry," *Journal of Low Temperature Physics*, vol. 197, pp. 348–356, Aug. 2019.

[31] S. S. Ustavshikov, Y. N. Nozdrin, M. Y. Levichev, A. V. Okomel'kov, I. Y. Pashenkin, P. A. Yunin, A. M. Klushin, and D. Y. Vodolazov, "Photoresponse of current-biased superconductor/normal metal strip with large ratio of resistivities," *Journal of Physics D: Applied Physics*, vol. 53, p. 395301, July 2020.

[32] O. Bourgeois, D. Tainoff, A. Tavakoli, Y. Liu, C. Blanc, M. Boukhari, A. Barski, and E. Hadji, "Reduction of phonon mean free path: From low-temperature physics to room temperature applications in thermoelectricity," *Comptes Rendus Physique*, vol. 17, pp. 1154–1160, Dec. 2016.